Elliptically polarised normal modes under conditions of nonstationary electromagnetically induced transparency

O.M. Parshkov

Abstract. **We report the results of numerical simulation of the evolution of a weak elliptically polarised input probe pulse in the case of electromagnetically induced transparency in the field of elliptically polarised control light. It is shown that the electric field strength of any input probe pulse can be represented as a sum of the electric field strengths of two subpulses whose polarisation ellipses have the same constant eccentricities and mutually perpendicular directions of the major axes, one of these axes being parallel to the major axis of the polarisation ellipse of the control light. The directions of rotation of the electric field strength vectors of subpulses are mutually opposite. Subpulses move with different velocities in a medium, which leads to their spatial separation. In the propagation of subpulses, their polarisation characteristics (eccentricities and directions of major axes of polarisation ellipses) remain unchanged. At any stage of evolution, including the instants of significant spatial overlapping of subpulses, the intensity of the probe light in the medium is the sum of their intensities. Consequently, these subpulses are nonstationary mutually orthogonal elliptically polarised normal modes of the probe field whose existence is related to the medium anisotropy caused by the control field. The simulation is carried out for a scheme of degenerate quantum transitions between $^3P_0$, $^3P_1^0$ and $^3P_2$ levels of the ^{208}Pb isotope, taking into account the Doppler broadening of the spectral lines under the assumption that the probe field has a higher frequency than the control field.**

Keywords: electromagnetically induced transparency, elliptic polarisation of light, birefringence, normal modes.

1. Introduction

Optical control of electromagnetic fields and populations of quantum-transition energy levels, based on the destructive interference of probability amplitudes under resonance excitation by the laser light, is of considerable interest in connection with the possibilities of its practical application. Depending on the specifics of the experiment, this control underlies a number of effects, the most significant of which are population trapping [1, 2] and electromagnetically induced transparency (EIT) [3–5]. Restricting ourselves to the EIT phenomenon, we note that its use is promising for the development of systems of optical quantum memory [4], systems of quantum

O.M. Parshkov Yuri Gagarin State Technical University of Saratov, ul. Politekhnicheskaya 77, 410054 Saratov, Russia;
e-mail: oparshkov@mail.ru

communications [4, 6, 7] and quantum information [3–5], and devices for high-precision magnetic measurements [8] and chronometry [9]. EIT lies at the basis of methods for producing large optical nonlinearities [5, 10] and amplification without population inversion [11, 12].

In the presence of a degeneracy of quantum-transition energy levels, EIT in a specific way manifests itself in the evolution of the polarisation characteristics of the interacting light fields. Thus, the authors of Refs [13, 14] studied theoretically and experimentally the EIT-accompanying rotation of the polarisation plane of the probe field with a change in the control light intensity, and the authors of Refs [15, 16] examined the effect of a constant magnetic field on the evolution of the circular components of the probe light. The linear and circular birefringence of the probe field in the case of EIT was investigated theoretically and experimentally in [17]. Theoretical work [18] predicted the possibility of propagating a probe EIT field in the form of two modes with different polarisation states.

In the above-mentioned works devoted to the study of the polarisation effects in EIT, the amplitudes of the probe and control fields were assumed to be stationary. This approach is valid for describing the quasi-stationary interaction of the waves, when the duration of the light pulses significantly exceed the times of irreversible relaxation of quantum transitions. Another situation, called the nonstationary EIT regime, arises if the probe pulse duration is less than the irreversible relaxation times or is comparable with them. It is this regime that is most promising from the point of view of the practical use of EIT in quantum communication and information systems. In [19, 20], a theoretical study was made of the propagation of the polarisation pulses of the probe field in the case of EIT in degenerate two-level quantum systems. It was found that the transfer of the light energy occurs at the speed of light in a vacuum, while the polarisation wave of the light propagates in a medium with a lower velocity. In work [21, 22], we studied theoretically the nonstationary EIT regime in the cases of linear and circular polarisations of the input control field in the Λ-scheme of degenerate quantum transitions. We showed that the birefringence arising under the action of the control light leads in the first case to the splitting of the circularly polarised input probe pulse into linearly polarised subpulses in the medium, while in the second case, the linearly polarised input probe pulse separates into circularly polarised components.

In this paper, we present the results of a numerical simulation of evolution of a weak short elliptically polarised probe pulse in the field of the elliptically polarised control light. The case of counterintuitive imposition [3] of interacting fields is considered. It is shown that birefringence in this situation

occurs at the frequency of the probe field, leading to the splitting of the input probe pulse into two elliptically polarised subpulses with identical eccentricities of the polarisation ellipses, but with different directions of rotation of the electric field strength vectors. Subpulses move in the medium without changing the polarisation state, and any probe pulse can be represented as the sum of subpulses propagating independently of each other. In other words, these subpulses are nonstationary normal modes of the probe light under EIT conditions in the field of the elliptically polarised control light.

Our theory takes into account the inhomogeneous broadening of the quantum-transition lines and does not use the weak probe field approximation, although the latter is assumed to be rather weak in comparison with the field of the control light. The calculations were carried out for a scheme of quantum transitions between the degenerate energy levels $^3P_0$, $^3P_2$, $^3P_1^0$ of the ^{208}Pb isotope, in the vapours of which the authors of Refs [23, 24] experimentally observed EIT of circularly polarised laser fields.

2. Formulation of the problem

The Λ-scheme underlying the further analysis consists of nondegenerate lower ($^3P_0$), fivefold degenerate middle ($^3P_2$) and triply degenerate upper ($^3P_1^0$) levels of the ^{208}Pb isotope. Let ϕ_κ ($k = 1, 2, ..., 9$) be an orthonormal basis of the common eigenfunctions of the operators of energy, square and projection of the angular momentum on the z axis for an isolated atom corresponding to the lower ($k = 1$, $M = 0$), upper ($k = 2, 3, 4$, $M = -1, 0, 1$) and middle ($k = 5, 6, ..., 9$, $M = -2, -1, 0, 1, 2$) levels. We denote by D_1 and D_2 the reduced electric dipole moments of the $^3P_0 \rightarrow {}^3P_1^0$ and $^3P_2 \rightarrow {}^3P_1^0$ transitions, respectively, and by ω_1 and ω_2 ($\omega_1 > \omega_2$) the frequencies of these transitions for an atom at rest. We also set $T_1 = 1/\Delta_1$, where Δ_1 is the half-width (at the e^{-1} level) of the density distribution of frequencies ω_1' of the $^3P_0 \rightarrow {}^3P_1^0$ transitions in view of the Doppler effect.

We define the electric field of two laser pulses propagating along the z axis, having carrier frequencies ω_1 and ω_2 (probe and control pulses, respectively), in the form

$$\boldsymbol{E} = \sum_{l=1}^{2} \mu_l [\boldsymbol{i}E_{xl}\cos(\omega_l t - k_l z + \delta_{xl})$$
$$+ \boldsymbol{j}E_{yl}\cos(\omega_l t - k_l z + \delta_{yl})], \tag{1}$$

where $\mu_l = \hbar\sqrt{2l + 1}/(|D_l|T_1)$; $\boldsymbol{i}$ and $\boldsymbol{j}$ are the unit vectors of the x and y axes; E_{xl}, E_{yl} are the nonnegative real amplitudes; δ_{xl} and δ_{yl} are the phase additions of the x- and y-components of the probe ($l = 1$) and control ($l = 2$) fields; and $k_l = \omega_l/c$. The quantities E_{xl}, E_{yl}, δ_{xl} and δ_{yl} are functions of z and t.

We define the variables f_l and g_l as

$$f_l = [E_{xl}\exp(\mathrm{i}\delta_{xl}) - \mathrm{i}E_{yl}\exp(\mathrm{i}\delta_{yl})]/\sqrt{2},$$

$$g_l = [E_{xl}\exp(\mathrm{i}\delta_{xl}) + \mathrm{i}E_{yl}\exp(\mathrm{i}\delta_{yl})]/\sqrt{2}.$$

Following [25], we henceforth refer to f_l and g_l as the amplitudes of the right- and left-hand circular field components, respectively, although the opposite terminology is often used (see e. g., [26]). We represent the wave function Ψ of an atom in an electric field (1) as an expansion in the basis of ϕ_k ($k = 1, 2, ..., 9$):

$$\Psi = \bar{c}_1\phi_1 + \left(\sum_{k=2}^{4}\bar{c}_k\phi_k\right)\exp(-\mathrm{i}\xi_1) + \left(\sum_{k=5}^{9}\bar{c}_k\phi_k\right)\exp[-\mathrm{i}(\xi_1 - \xi_2)],$$

where $\xi_l = \omega_l t - k_l z$, $l = 1, 2$. We introduce the quantities

$$c_1 = p_1^*\bar{c}_1, \ \ c_2 = \bar{c}_2, \ \ c_4 = \bar{c}_4, \ \ c_5 = p_2\bar{c}_5,$$

$$c_7 = (1/\sqrt{6})p_2\bar{c}_7, \ \ c_9 = p_2\bar{c}_9, \tag{2}$$

where $p_l = 2D_l/|D_l|$ and $l = 1, 2$. We define the normalised independent variables s and w as

$$s = z/z_0, \ \ w = (t - z/c)/T_1,$$

where $z_0 = 3\hbar c/(2\pi N|D_1|^2 T_1\omega_1)$ and N is the concentration of atoms. Using the Maxwell and Schrödinger equations, we obtain in the first approximation of slow envelopes the system of equations:

$$\frac{\partial f_1}{\partial s} = \frac{\mathrm{i}}{\sqrt{\pi}}\int_{-\infty}^{+\infty} c_1 c_2^*\exp(-\varepsilon_1^2)\,\mathrm{d}\varepsilon_1,$$

$$\frac{\partial f_2}{\partial s} = -\frac{\mathrm{i}}{\sqrt{\pi}}\xi\int_{-\infty}^{+\infty}(c_4^* c_9 + c_2^* c_7)\exp(-\varepsilon_1^2)\,\mathrm{d}\varepsilon_1,$$

$$\frac{\partial g_1}{\partial s} = -\frac{\mathrm{i}}{\sqrt{\pi}}\int_{-\infty}^{+\infty} c_1 c_4^*\exp(-\varepsilon_1^2)\,\mathrm{d}\varepsilon_1,$$

$$\frac{\partial g_2}{\partial s} = \frac{\mathrm{i}}{\sqrt{\pi}}\xi\int_{-\infty}^{+\infty}(c_2^* c_5 + c_4^* c_7)\exp(-\varepsilon_1^2)\,\mathrm{d}\varepsilon_1,$$

$$\frac{\partial c_1}{\partial w} = -\mathrm{i}(f_1 c_2 - g_1 c_4),$$

$$\frac{\partial c_2}{\partial w} + \mathrm{i}\varepsilon_1 c_2 = -\frac{\mathrm{i}}{4}(f_1^* c_1 + g_2^* c_5 - f_2^* c_7) - \gamma c_2, \tag{3}$$

$$\frac{\partial c_4}{\partial w} + \mathrm{i}\varepsilon_1 c_4 = \frac{\mathrm{i}}{4}(g_1^* c_1 - g_2^* c_7 + f_2^* c_9) - \gamma c_4,$$

$$\frac{\partial c_5}{\partial w} + \mathrm{i}(\varepsilon_1 - \varepsilon_2)c_5 = -\mathrm{i}g_2 c_2,$$

$$\frac{\partial c_7}{\partial w} + \mathrm{i}(\varepsilon_1 - \varepsilon_2)c_7 = \frac{\mathrm{i}}{6}(f_2 c_2 - g_2 c_4),$$

$$\frac{\partial c_9}{\partial w} + \mathrm{i}(\varepsilon_1 - \varepsilon_2)c_9 = \mathrm{i}f_2 c_4,$$

where

$$\varepsilon_1 = (\omega_1' - \omega_1)/\Delta_1, \ \ \varepsilon_2 = \beta\varepsilon_1,$$

$$\xi = 0.6\beta|D_2/D_1|^2, \ \ \beta = \omega_2/\omega_1. \tag{4}$$

The system of equations (3) does not contain the amplitudes $\bar{c}_3$, $\bar{c}_6$ and $\bar{c}_8$, which agrees with the selection rules ($\Delta M = \pm 1$) for transitions under the action of the circular field components (1). In the equations for c_2 and c_4, the terms $-\gamma c_2$ and $-\gamma c_4$ are introduced phenomenologically to take into account the spontaneous decay of the upper-level states of the Λ-scheme in question. Here $\gamma = T_1/(2\tau)$, where τ is the radiative lifetime of the $^3P_1^0$ level. The allowance for the Doppler broadening of the quantum-transition lines by averaging the dipole moments of the atoms with respect to the parameter ε_1,

determined in (4), led to the appearance of integrals in the first four equations of system (3).

To describe the light, we use the parameters a_l, α_l, γ_l of polarisation ellipses of the probe ($l = 1$) and control ($l = 2$) light. Here a_l is the semi-major axis of the ellipse measured in μ_l units; α_l is the angle of its inclination to the x axis in radians; and γ_l is the contraction parameter ($0 \leqslant \alpha_l < \pi$, $-1 \leqslant \gamma_l \leqslant +1$) [25]. The quantity $|\gamma_l|$ determines the ratio of the minor axis of the ellipse to its major axis. The condition $\gamma_l = 1$ ($\gamma_l = -1$) means $\sigma_-(\sigma_+)$ polarisation. If $|\gamma_l| = 1$, then the angle α_l is not defined, and in the calculations we formally assume it to be equal to -0.1 rad.

In carrying out a numerical analysis, the boundary conditions describing the probe light at the input surface $s = 0$ of the resonant medium were chosen in the form

$$\alpha_1 = \alpha_{10}, \quad a_1 = a_{10}, \quad \gamma_1 = \gamma_{10}, \quad \delta_{x1} = \delta_{x10} \tag{5}$$

($w \geqslant 0$), and the input control light is given by the relations

$$\alpha_2 = \alpha_{20}, \quad a_2 = a_{20}, \quad \gamma_2 = \gamma_{20}, \quad \delta_{x2} = \delta_{x20}, \tag{6}$$

where α_{l0}, γ_{l0}, δ_{xl0} ($l = 1, 2$) and a_{20} are some constants. On the contrary, a_{10}, which is the semi-major axis of the polarisation ellipse of the input probe field, was assumed to depend on the time w. As initial conditions, it was assumed that only the lower energy level is populated before the arrival of the probe pulse ($w < 0$), so that for $w = 0$ the equality $c_1 = 2$ is satisfied, and all other probability amplitudes given by expressions (2) are zero.

The form of the dependence of a_{10} on w was chosen so that equalities (5) describe a bell-shaped pulse of the probe light. Equations (6) describe the input control light, whose intensity does not change during the entire process of wave interaction. Such a model corresponds to the scheme of counterintuitive superposition of the control field, usually used in the experimental study of the EIT phenomenon [3].

According to [27], for the selected ^{208}Pb transitions, in formulas (3) and (4) $\omega_2/\omega_1 = 0.7$, $\xi = 2.11$ and (at $T = 900-1000$ K), $\gamma = 1.5 \times 10^{-2}$. In the case of $T = 950$ K, we have $T_1 = 1.63 \times 10^{-10}$ s. Choosing saturated vapours of ^{208}Pb for estimates and using the data of [28], we find $N = 3.4 \times 10^{13}$ cm^{-3} and $z_0 = 0.03$ cm at the same temperature. Note that the value of z_0 depends strongly on temperature. Thus, $z_0 = 0.1$ cm at 900 K, and $z_0 = 0.01$ cm at 1000 K. The time T_1 depends weakly on the temperature, decreasing with its change by about 5%. The time τ of the radiative decay of the $^3P_1^0$ level, which plays at low vapour densities the role of the irreversible relaxation time of the quantum system, is about 6 ns [27].

Then, use is made of dimensionless intensities of I_l, i.e. densities of energy fluxes of the probe ($l = 1$) and control ($l = 2$) fields, measured in units of $c\mu_1^2/(8\pi)$:

$$I_1 = a_1^2(1 + \gamma_1^2), \quad I_2 = (\beta/\xi)a_2^2(1 + \gamma_2^2).$$

The dimensional intensities $\bar{I}_l$ (in kW cm^{-2}) of the probe and control fields in the temperature range $900-1000$ K (this range is used for dimensional measurements) can be defined as $\bar{I}_l = 1.3I_l$. Note that the system of equations (3) is valid for any ratio of the intensities of the control and probe fields. However, below we describe EIT under the condition $I_{10} \ll I_{20}$, i.e., in the regime when the input probe light is much weaker than the control field.

3. Normal modes (results of numerical analysis)

We set in (5) and (6)

$$\alpha_{10} = \pi/6, \quad a_{10} = 0.2\,\mathrm{sech}\,[(w - 20)/5],$$
$$\gamma_{10} = -0.5, \quad \delta_{x10} = 0; \tag{7}$$

$$\alpha_{20} = 0, \quad a_{20} = 6.6516, \quad \gamma_{20} = -0.3, \quad \delta_{x20} = 0. \tag{8}$$

Boundary conditions (7) describe a 1.5-ns input probe pulse with a peak intensity $\bar{I}_1 = 65$ W cm^{-2}. This probe light is polarised elliptically with a contraction parameter equal to -0.5 (left-hand elliptic polarisation [25]), where the angle between the major axis of its polarisation ellipse and the x axis is equal to $\pi/6$. According to (8), the constant intensity I_2 of the control light is approximately 20 kW cm^{-2} (the intensity of the control light in experimental studies [23, 24] was approximately the same). Since $\bar{I}_2$ exceeds $\bar{I}_1$ by more than 300 times, the situation described by formulas (7) and (8) refers to the case of the weak probe light. The control field also has the left-hand elliptical polarisation with a contraction parameter equal to -0.3, the major axis of the polarisation ellipse coinciding with the x axis. The latter is assumed for simplicity in all subsequent calculations and does not limit the generality of the reasoning, since the evolution of the interacting fields depends only on the angle between the major axes of their polarisation ellipses. Note that in the slow-envelope approximation, a large difference between the carrier frequencies of the probe and control fields leads to the independence of the characteristics of the polarisation ellipse of the control light in the medium from the values of the constant quantities δ_{x10} and δ_{x20}.

The results of the calculation are shown in Fig. 1. The plots of the dependence of I_1 on w for different fixed distance s (thick curves in Fig. 1) show that at sufficiently small distances inside the medium, the input probe pulse begins to split into two separate subpulses (pulses 1 and 2 in Figs 1b and 1c). In this case, the form of dashed and thin curves describing the evolution of the quantities α_1 and γ_1, respectively, indicates that as the probe field passes through a given point of space, the angle α_1 smoothly changes from 0 to about $\pi/2$, while γ_1 smoothly decreases from a value approximately equal to 0.74 to a value close to -0.74 (the dashed and thin curves are shown here and below only in those time intervals where the value of I_1 differs appreciably from zero). Thus, at short distances, the polarisation state of the probe field, determined by the values of α_1 and γ_1, varies as the pulse propagates in the medium.

At sufficiently large values of s, the energy of the probe light is concentrated in two subpulses (1 and 2 in Fig. 1d). In the region of localisation of each of these pulses, the polarisation characteristics of the light remain unchanged both in space and time. For pulse 1, calculation yields $\alpha_1 = 0$, $\gamma_1 = 0.7415$, and for pulse 2 we have $\alpha_1 = \pi/2$, $\gamma_1 = -0.7415$. This circumstance allows us to assume that pulses 1 and 2 are normal modes (waves) [26] of the probe light. In an anisotropic crystalline medium, normal modes are linearly polarised, and in an optically active medium they have circular polarisation. In our case, when the optical isotropy of the gas is removed by imposing the elliptically polarised control light, the normal modes are elliptically polarised in the general case.

In what follows, the normal mode (corresponding to pulse 1 in Fig. 1d) for which $\alpha_1 = 0$ will be called the parallel mode,
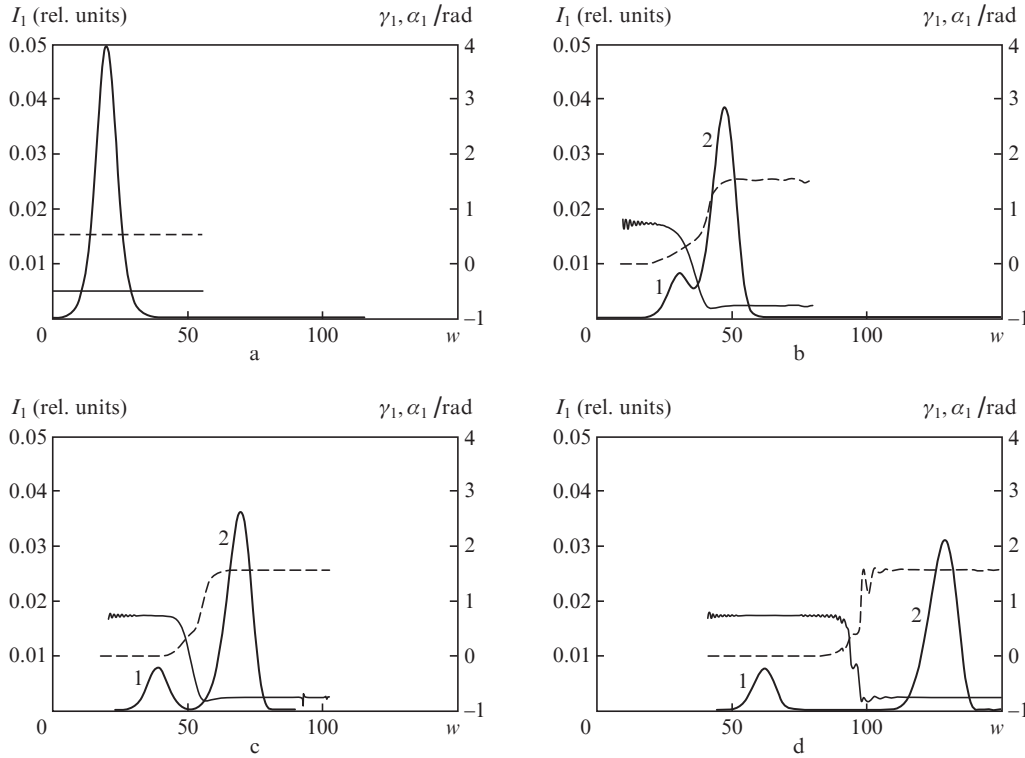
Figure 1. Evolution of the characteristics of the probe field in the medium for $s =$ (a) 0, (b) 100, (c) 180 and (d) 400 (I_1 – thick curves, α_1 and γ_1 – dashed and thin curves, respectively); $\gamma_{20} = -0.3$.

and the normal mode for which $\alpha_1 = \pi/2$ will be called the perpendicular mode. Note that the parallel mode propagates faster than the perpendicular mode. If we denote by v the velocity of the normal mode, then under the conditions in question $c/v \approx 16$ and $c/v \approx 40$ for the parallel mode and the perpendicular mode, respectively.

The curves describing the evolution of the phase δ_{x1} of the probe field in the medium are not presented in Fig. 1. In this regard, we note that in the region of each of the subpulses, in which the energy of the probe field is concentrated at large distances, this quantity is independent of s and w. For a subpulse corresponding to the parallel normal mode, $\delta_{x1} = -0.5001$, and for a subpulse corresponding to the perpendicular normal mode, $\delta_{x1} = 0.2852$.

Figure 2 shows the calculation results, the initial conditions of which differ from (7), (8) only in that $\gamma_{20} = 0.3$. This choice means the right-hand elliptic polarisation of the control field, whereas in the previous calculation the polarisation was left-handed. It follows from Figs 2b and 2c that at small distances, as in the case of left-hand polarisation, the probe pulse splits into two subpulses, and during this process the major axis of the polarisation ellipse rotates by an angle approximately equal to $\pi/2$ (dashed curves in Figs 2b and 2c). However, the direction of variation in γ_1 is opposite to that of $\gamma_{20} = -0.3$. According to the plots (thin curves in Figs 2b and 2c), this value varies smoothly from about -0.74 to 0.74. At large distances, the energy of the probe light is concentrated in two pulses (Fig. 2d) with unchanged polarisation states. In the region of pulse 1, $\alpha_1 = 0$, $\gamma_1 = -0.7415$, and in the region of pulse 2, $\alpha_1 = \pi/2$, $\gamma_1 = 0.7415$. Thus, pulse 1 is the parallel normal mode, and pulse 2 is the perpendicular normal mode.

Using the results given above, we can make the following assumption. The contraction parameters of polarisation ellipses

of parallel and perpendicular normal modes can be represented in the form $\gamma_1 = -\text{sgn}(\gamma_2)\bar{\gamma}_1$ and $\gamma_1 = \text{sgn}(\gamma_2)\bar{\gamma}_1$, respectively, where $\bar{\gamma}_1 \geqslant 0$ is the modulus of the contraction parameters, which is the same for both modes, and $\text{sgn}(x)$ is a sign function equal to -1 for $x < 0$, to zero for $x = 0$ and $+1$ for $x > 0$; $\bar{\gamma}_1 = 0.7415$ (for the situations under study).

On the basis of physical considerations, we can assume that $\bar{\gamma}_1$ depends only on $|\gamma_2|$, i.e. the modulus of the contraction parameter of the polarisation ellipse of the control light. This circumstance was confirmed by a series of calculations for various values of the quantities (including the temporal shape of the envelope of the input probe field) entering into boundary conditions (5) and (6). Figure 3 shows the results of calculations performed under conditions

$$\alpha_{10} = \pi/3, \quad a_{10} = \sqrt{0.08}\,\text{sech}[(w - 200)/50],$$
$$\gamma_{10} = 0, \quad \delta_{x10} = 0; \tag{9}$$

$$\alpha_{20} = 0, \quad a_{20} = 5.7606, \quad \gamma_{20} = -0.3, \quad \delta_{20} = 0. \tag{10}$$

In this case, the input probe pulse is linearly polarised at an angle of $\pi/3$ to the x axis. It has a 10-fold longer duration and a 1.6-fold greater peak intensity than the probe pulses in the previous calculations (see Figs 1a and 2a); the intensity of the control field is ~ 15 kW cm^{-2}, i.e., 75% of I_2 corresponding to conditions (8). A qualitative picture of the process of the splitting of the input probe pulse into normal modes is analogous to that shown in Fig. 1, although now such a splitting requires a much larger distance (the jump in α_1 in Fig. 3d is determined by the choice of the region of variation of this quantity). At a distance $s = 4000$ (Fig. 3d), the calculation shows that the value of $\bar{\gamma}_1$ with an error of less than 0.1%
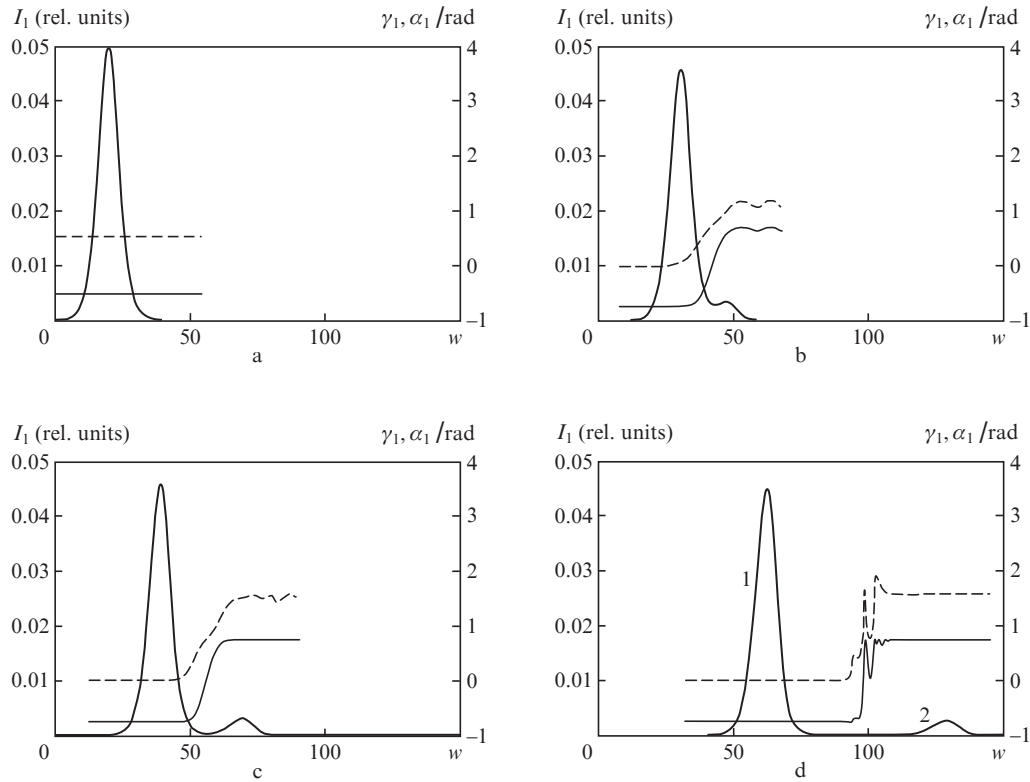
Figure 2. Evolution of the quantities I_1, α_1 and γ_1 in the medium for $s = $ (a) 0, (b) 100, (c) 180 and (d) 400 (the notation is the same as in Fig. 1); $\gamma_{20} = 0.3$.
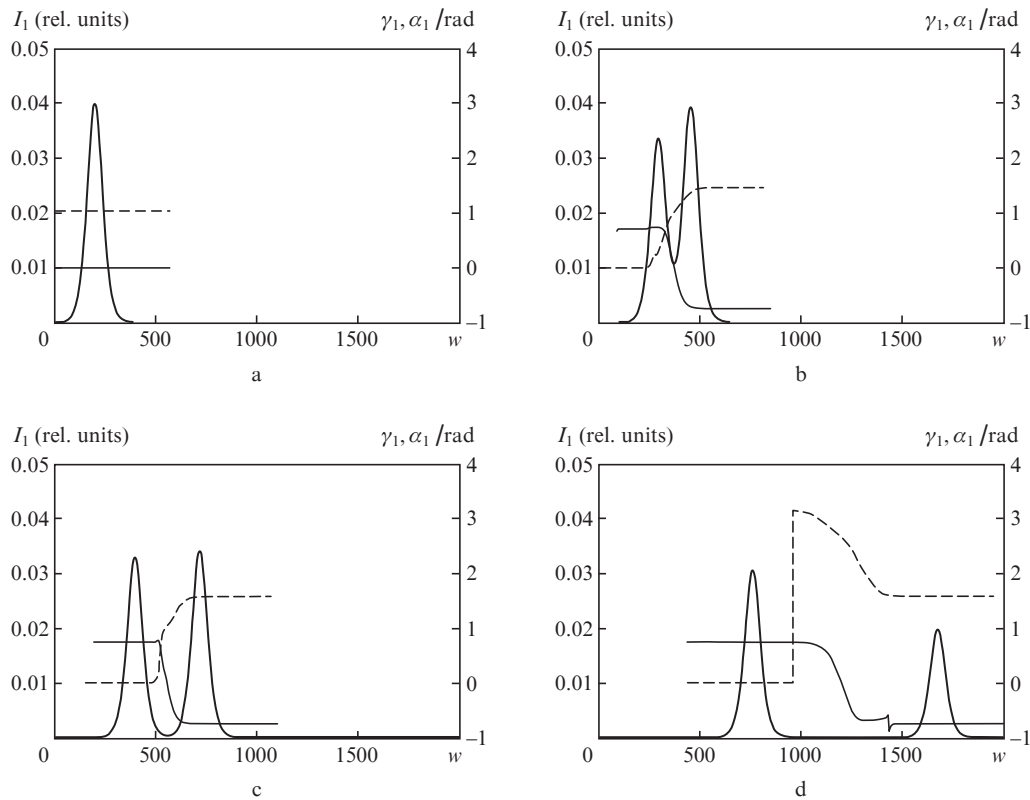
Figure 3. Evolution of the quantities I_1, α_1 and γ_1 in the medium for $s = $ (a) 0, (b) 700, (c) 1400 and (d) 4000 (the notation is the same as in Fig. 1); $\gamma_{20} = -0.3$.

coincides with the value obtained in the first two calculations. The error is due not only to the error of the numerical method for solving system (3), but also to the fact that this system of equations takes into account the influence of the probe field on the control field.

The dependence of $\bar{\gamma}_1$ on $|\gamma_2|$, constructed from the results of calculations similar to the first calculation of this section, is shown in Fig. 4. One can see that the normal modes of the probe light have linear and circular polarisations in the case of linear and circular polarisations of the control field, respectively. This circumstance corresponds to the conclusions of papers [21, 22]. When $|\gamma_2|$ changes near zero, the parameter $\bar{\gamma}_1$ changes faster than $|\gamma_2|$, and the situation is opposite when the value of $|\gamma_2|$ is equal to unity.
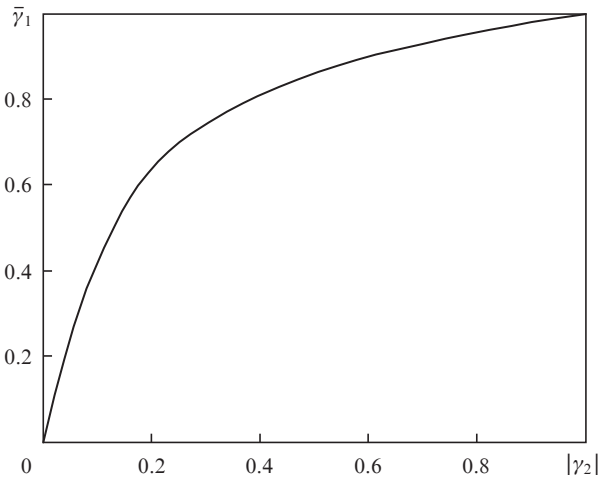
Figure 4. Dependence of $\bar{\gamma}_1$ on $|\gamma_2|$.

Note that if we set $a_{20} = 0$ in (8), which corresponds to the absence of the control light, then, as calculation shows, the energy of the input probe pulse is almost completely absorbed by the medium at a distance $s = 3$ from the input surface. The fact that upon imposing the control light this energy penetrates into the medium at a distance $s = 400$ (see, for example, Fig. 1d) indicates the presence of the EIT phenomenon.

4. Representation of the probe field by a superposition of normal modes

The probe field, expressed by formula (1), can be represented as the sum of normal modes. Using standard definitions of the polarisation ellipse parameters [25], we obtain the following relations between the variables entering into (1) and the parameters of the polarisation ellipse of the probe wave:

$$E_{x1} = a_1\varepsilon_+(\alpha_1,\gamma_1), \quad E_{y1} = a_1\varepsilon_-(\alpha_1,\gamma_1),$$

$$\varepsilon_+(\alpha_1,\gamma_1) = \sqrt{[1 + \gamma_1^2 + (1 - \gamma_1^2)\cos 2\alpha_1]/2},$$

$$\varepsilon_-(\alpha_1,\gamma_1) = \sqrt{[1 + \gamma_1^2 - (1 - \gamma_1^2)\cos 2\alpha_1]/2},$$

$$\delta_{y1} = \delta_{x1} + \delta_1, \quad \delta_1 = \begin{cases} \arg p, & p \neq 0, \\ 0, & p = 0, \end{cases}$$

$$p = (1 - \gamma_1^2)\sin 2\alpha_1 + 2\gamma_1 i.$$

(11)

(12)

Expressions (11) and (12) show that the values of α_1, a_1, γ_1 and δ_{x1} uniquely determine the probe field (as well as the values of E_{x1}, E_{y1}, δ_{x1} and δ_{y1}).

We denote by J_x and J_y the x- and y-components of the Jones vector [26] of the probe wave:

$$J_x = \mu_1 E_{x1}\exp(i\delta_{x1}), \quad J_y = \mu_1 E_{y1}\exp(i\delta_{y1}). \tag{13}$$

We use the symbols $\alpha_1^{(i)}$, $a_1^{(i)}$, $\gamma_1^{(i)}$, $\delta_{x1}^{(i)}$ and $\delta_{y1}^{(i)}$ for the quantities α_1, a_1, γ_1, δ_{x1} and δ_{y1}, describing parallel ($i = 1$) and perpendicular ($i = 2$) normal modes of the probe field. According to what was said in the previous section, we can write

$$\alpha_1^{(1)} = 0, \quad a_1^{(1)}, \quad \gamma_1^{(1)} = -\text{sgn}(\gamma_2)\bar{\gamma}_1, \quad \delta_{x1}^{(1)},$$

$$\delta_{y1}^{(1)} = \delta_{x1}^{(1)} - \text{sgn}(\gamma_2)\pi/2,$$

(14)

$$\alpha_1^{(2)} = \pi/2, \quad a_1^{(2)}, \quad \gamma_1^{(2)} = \text{sgn}(\gamma_2)\bar{\gamma}_1, \quad \delta_{x1}^{(2)},$$

$$\delta_{y1}^{(2)} = \delta_{x1}^{(2)} + \text{sgn}(\gamma_2)\pi/2,$$

(15)

where $a_1^{(i)}$ is the s- and w-dependent semi-major axis of the polarisation ellipse of parallel ($i = 1$) and perpendicular ($i = 2$) normal modes, while all other quantities are independent of s and w. Using formulas (11), (12) and (13), we find expressions for the components $J_x^{(i)}$ and $J_y^{(i)}$ of the Jones vectors of parallel ($i = 1$) and perpendicular ($i = 2$) normal modes:

$$J_x^{(1)} = \mu_1 a_1^{(1)}\exp(i\delta_{x1}^{(1)}), \quad J_y^{(1)} = \mu_1\bar{\gamma}_1 a_1^{(1)}\exp(i\delta_{y1}^{(1)}), \tag{16}$$

$$J_x^{(2)} = \mu_1\bar{\gamma}_1 a_1^{(2)}\exp(i\delta_{x1}^{(2)}), \quad J_y^{(2)} = \mu_1 a_1^{(2)}\exp(i\delta_{y1}^{(2)}). \tag{17}$$

Using (16) and (17) together with the expressions for $\delta_{y1}^{(i)}$ from formulas (14) and (15), it is not difficult to establish the orthogonality condition for the Jones vectors of normal modes:

$$J_x^{(1)}J_x^{(2)*} + J_y^{(1)}J_y^{(2)*} = 0. \tag{18}$$

Thus, the parallel and perpendicular normal modes of the probe field form an orthogonal pair, and any probe field of form (1) can be represented as the sum of such modes [26]. Thus, it is sufficient to express the characteristics of the normal modes on the input surface $s = 0$ in (14) and (15) through similar characteristics of the input probe pulse; in this case, $\gamma_1^{(1)}$ and $\gamma_1^{(2)}$ are assumed to be known on the basis of a numerical definition of $\bar{\gamma}_1$ (see Fig. 4). Thus, only $a_{10}^{(i)}$ and $\delta_{x10}^{(i)}$ ($i = 1, 2$) should be defined, i.e. the values of the quantities $a_1^{(i)}$ and $\delta_{x1}^{(i)}$ on the input surface.

In the considered cases of absence of phase modulation of the input probe field, δ_{x10} does not depend on w and, without loss of generality, is assumed below to be zero. Equating the Jones vector of the probe wave incident on the input surface to the sum of the Jones vectors of the normal modes on this surface, we arrive at the system of equations:

$$\begin{cases} X + \bar{\gamma}_1 Z = A, \quad Y + \bar{\gamma}_1 T = 0, \\ \bar{\gamma}_1 Y - T = B, \quad \bar{\gamma}_1 X - Z = C, \end{cases} \tag{19}$$

where the unknown quantities X, Y, Z, T and the known quantities A, B, C are given by formulas

$$X = (a_{10}^{(1)}/a_{10})\cos\delta_{x10}^{(1)}, \quad Y = (a_{10}^{(1)}/a_{10})\sin\delta_{x10}^{(1)},$$

$$Z = (a_{10}^{(2)}/a_{10})\cos\delta_{x10}^{(2)}, \quad T = (a_{10}^{(2)}/a_{10})\sin\delta_{x10}^{(2)}; \tag{20}$$

$$A = \varepsilon_+(\alpha_{10}, \gamma_{10}), \quad B = \mathrm{sgn}(\gamma_2)\varepsilon_-(\alpha_{10}, \gamma_{10})\cos\delta_{10},$$

$$C = -\mathrm{sgn}(\gamma_2)\varepsilon_-(\alpha_{10}, \gamma_{10})\sin\delta_{10}. \tag{21}$$

The discriminant of the linear system of equations (19) is $-(1 + \gamma_{10}^2)^2 \neq 0$, and, consequently, this system has a unique solution. The coefficients in (19) for unknowns and the right-hand sides of the equations described by formulas (21) are independent of w, so that the components X, Y, Z, T of the solution of the system also do not depend on w. The missing values of the characteristics of normal modes are further defined as follows:

$$a_{10}^{(1)} = a_{10}\sqrt{X^2 + Y^2}, \quad a_{10}^{(2)} = a_{10}\sqrt{Z^2 + T^2},$$

and then, on the basis of formulas (20), the values of $\delta_{x10}^{(i)}$ are found.

Using this procedure for normal modes corresponding to the input probe field of the first of the above-presented calculations, one can obtain the characteristics:

$$\alpha_{10}^{(1)} = 0, \quad a_{10}^{(1)} = 0.0720\,\mathrm{sech}[(w - 20)/5],$$

$$\gamma_{10}^{(1)} = 0.7415, \quad \delta_{x10}^{(1)} = -0.4991, \tag{22}$$

$$\alpha_{10}^{(2)} = \pi/2, \quad a_{10}^{(2)} = 0.1646\,\mathrm{sech}[(w - 20)/5],$$

$$\gamma_{10}^{(2)} = -0.7415, \quad \delta_{x10}^{(2)} = 0.2865. \tag{23}$$

We note the practical agreement between the values of $\delta_{x10}^{(1)}$ and $\delta_{x10}^{(2)}$ with the values obtained for the normal modes of the first calculation. The results of calculations using data (22), (23) together with the conditions (8) for the input control light are shown in Fig. 5 and demonstrate the evolution of both normal modes in the medium.

The parallelism of the time axis of lines (2) and (3) and the height of their position that is independent of the distance s (Figs 5a–5d) indicate that the polarisation characteristics α_1 and γ_1 of each normal mode remain unchanged when it propagates in the medium. This property is included in the standard definition of normal modes. The sum of the intensities of the normal modes at each distance s coincides (with an accuracy of about 0.2 %) with the intensity of the probe field of the first calculation. This circumstance is illustrated in Fig. 6.

The procedure for finding the characteristics of normal modes using Eqn (20) is applicable under the condition $\gamma_2 \neq 0$. For $\gamma_2 = 0$, as noted above, $\bar{\gamma}_1 = 0$, i.e., the normal modes represent the linearly polarised light. It can be shown that in this case their characteristics on the input surface are defined as

$$\alpha_{10}^{(1)} = 0, \quad a_{10}^{(1)} = a_{10}\varepsilon_+(\alpha_{10}, \gamma_{10}), \quad \gamma_{10}^{(1)} = 0, \quad \delta_{x10}^{(1)} = 0,$$

$$\alpha_{10}^{(1)} = \pi/2, \quad a_{10}^{(1)} = a_{10}\varepsilon_-(\alpha_{10}, \gamma_{10}), \quad \gamma_{10}^{(2)} = 0, \quad \delta_{x10}^{(2)} = \delta_1,$$

where δ_1 is given by (12) for $\alpha_1 = \alpha_{10}$ and $\gamma_1 = \gamma_{10}$.
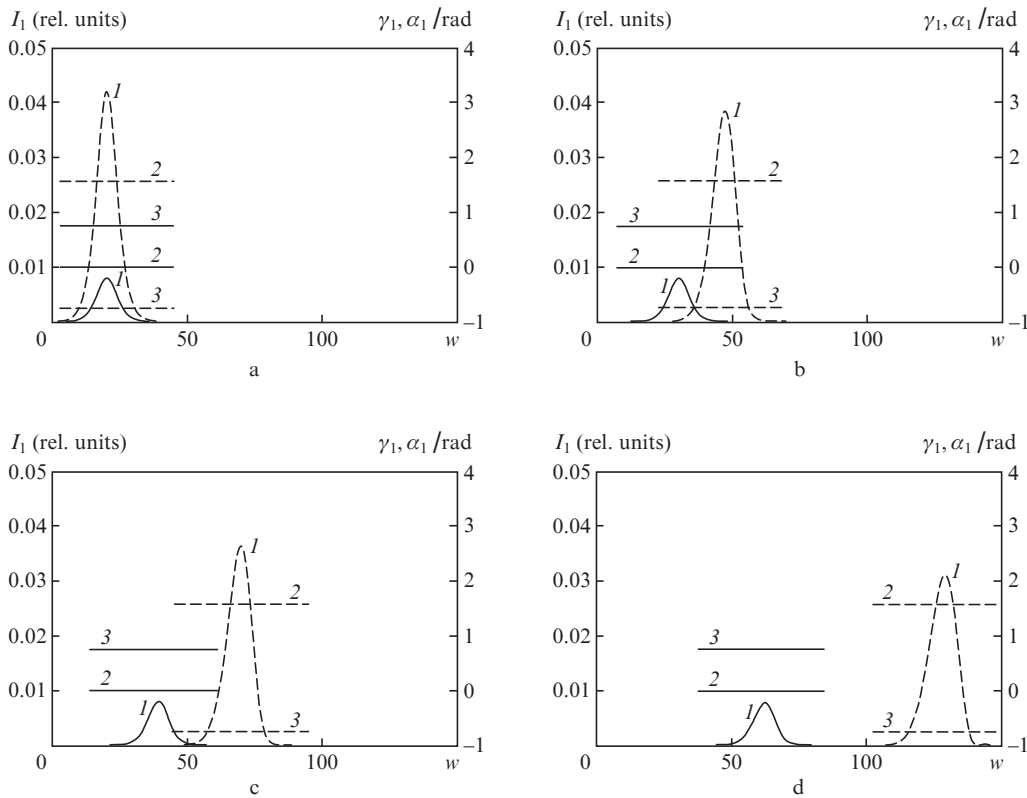
Figure 5. Calculated characteristics (1) I_1, (2) α_1 and (3) γ_1 of parallel (solid curves) and perpendicular (dashed curves) normal modes for the distances $s =$ (a) 0, (b) 100, (c) 180 and (d) 400.

I_1 (rel. units)

a

I_1 (rel. units)

b
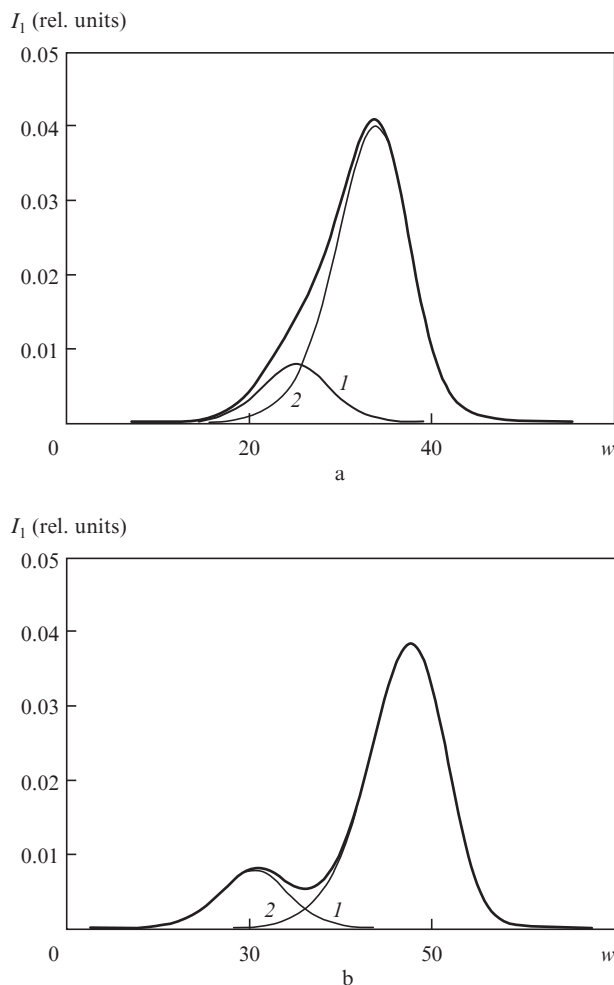
Figure 6. Intensities of the probe field (thick curves) of (*1*) parallel and (*2*) perpendicular normal modes at s = (a) 50 and (b) 100.

5. Conclusions

The results of the calculations show that in the case of EIT, in the field of elliptically polarised control light, the gaseous medium acquires the ability of birefringence with elliptically polarised normal modes of the probe field. Note that birefringence with normal modes of this type takes place in the propagation of radio waves in a magnetised cosmic plasma [29]. The major axis of the polarisation ellipse of one of the normal modes of the probe field is parallel to the major axis of the polarisation ellipse of the control light, while the major axis of the polarisation ellipse of the other normal mode is perpendicular to it. The ratio of the minor axis to the major axis is the same for the polarisation ellipses of both modes. The direction of rotation of the electric field strength vector of the first of these modes is opposite to the direction of rotation of the electric field strength vector of the control light. The vector of the electric field strength of the other mode rotates in the same direction as the corresponding vector of the control field. The pulse of the first-type mode propagates in the medium slower than the pulse of the second-type mode. The polarisation characteristics of both modes are determined only by the polarisation characteristics of the control field.

It is shown that each normal mode of the probe light propagates in a medium without changing the polarisation state and independently of the other mode. The electric field

strength of an arbitrary probe pulse in a medium can be represented as the sum of the field strengths of normal modes, and the intensity of an arbitrary probe pulse can be represented in the same way. These properties of the light are usually implied when using the term 'normal mode' [26].

The difference in the velocities of pulses associated with normal modes leads to a separation of an arbitrary input pulse in the medium into two subpulses, each representing one normal mode. At the initial stage of the decay of the probe pulse, the 'runaway' of its normal modes is manifested in a significant temporal and spatial dependence of its polarisation characteristics.

Kis et al. [18] studied theoretically the stationary EIT regime in the same scheme of quantum transitions as in the present paper. However, Kis et al. [18] assumed that the control field acts on the short-wavelength transition, and the probe field on the long-wavelength transition. The boundary and initial conditions used by us correspond to the opposite situation. In our case, both normal modes propagate in the medium without absorption, whereas in [18] the absorption of one of the normal modes was significant.

In conclusion, we note that the study of the nonstationary polarisation effects accompanying EIT is, from a practical point of view, promising for designing devices whose operation principle is based on controlling the polarisation state of coherent optical light.

References

1. Agap'ev B.D., Gornyi M.B., Matisov B.G., Rozhdestvenskii Yu.V. *Usp. Fiz. Nauk*, **163**, 1 (1993).
2. Vitanov N.V., Rangelov A.A., Shore B.W., Bergmann K. *Rev. Mod. Phys.*, **89**, 015006 (2017).
3. Harris S.E. *Phys. Today*, **50**, 36 (1997).
4. Lukin M.D. *Rev. Mod. Phys.*, **75**, 457 (2003).
5. Fleischhauer M., Imamoğlu A., Marangos J.P. *Rev. Mod. Phys.*, **77**, 633 (2005).
6. Duan L.-M., Lukin M.D., Cirac J.I., Zoller P. *Nature (London)*, **414**, 413 (2001).
7. Sinatra A. *Phys. Rev. Lett.*, **97**, 253601 (2006).
8. Martinalli M., Valente P., Failache H., Felinto D., Cruz L.S., Nussenzveig P., Lezama A. *Phys. Rev. A*, **69**, 043809 (2004).
9. Godone A., Micallilizio S., Levi F. *Phys. Rev. A*, **66**, 063807 (2002).
10. Lukin M.D., Imamoğlu A. *Nature (London)*, **413**, 273 (2001).
11. Kocharovskaya O., Mandel P. *Phys. Rev. A*, **42**, 523 (1990).
12. Popov A.K. *Izv. Akad. Nauk, Ser. Fiz.*, **60**, 99 (1996).
13. Wielandy S., Gaeta A.L. *Phys Rev. Lett.*, **81**, 3359 (1998).
14. Bo Wang, Shujing Li, Jie Ma, Hai Wang, Peng K.C., Min Xiao. *Phys. Rev. A*, **73**, 051801(R) (2006).
15. Agarwal G.S., Shubhrangshu Dasgupta. *Phys. Rev. A*, **67**, 023814 (2003).
16. Sautenkov V.A., Rostovtsev Y.V., Chen H., Hsu P., Agarwal G.S., Scully M.O. *Phys. Rev. Lett.*, **94**, 233601 (2005).
17. Tai Hyun Yoon, Chang Yong Park, Sung Jong Park. *Phys. Rev. A*, **70**, 061803(R) (2004).
18. Kis Z., Demeter G., Janszky J. *J. Opt. Soc. Am. B*, **30**, 829 (2013).
19. Zelenskii I.V., Mironov V.A. *Zh. Eksp. Teor. Fiz.*, **121**, 1068 (2002).
20. Yudin V.I., Basalaev M.Yu., Brazhnikov D.V., Taichenachev A.V. *Phys. Rev. A*, **88**, 023862 (2013).
21. Parshkov O.M. *Quantum Electron.*, **41**, 1010 (2011) [*Kvantovaya Elektron.*, **41**, 1010 (2011)].
22. Parshkov O.M. *Quantum Electron.*, **45** (11), 1010 (2015) [*Kvantovaya Elektron.*, **45** (11), 1010 (2015)].
23. Kasapi A., Maneesh J., Yin G.Y., Harris S.E. *Phys. Rev. Lett.*, **74**, 2447 (1995).
24. Maneesh J., Kasapi A., Yin G.Y., Harris S.E. *Phys. Rev. Lett.*, **75**, 4385 (1995).
25. Born M., Wolf E. *Principles of Optics* (Oxford: Pergamon Press, 1975; Moscow: Nauka, 1970).

26. Saleh B., Teich M. *Fundamentals of Photonics* (New York: Wiley, 1991).
27. De Zafra R.L., Marshall A. *Phys. Rev.*, **170**, 28 (1968).
28. Grigoriev I.S., Meilikhov E.Z. (Eds) *Handbook of Physical Quantities* (Boca Raton, NY: CRC Press, 1996; Moscow: Energoatomizdat, 1991).
29. Longair M. *High Energy Astrophysics* (Cambridge: Cambridge University Press, 2011; Moscow: Mir, 1983).